ELSEVIER

Biophysical Chemistry 114 (2005) 13–20

Biophysical Chemistry

http://www.elsevier.com/locate/biophyschem

NMR spectroscopic, mass spectroscopic, X-ray crystallographic, and theoretical studies of molecular mechanics of natural products: farformolide B and sesamin

Tiane-Jye Hsieh[a], Li-Hwa Lu[b], Chia-Ching Su[c,*]

[a]*Basic Medical Science Education Center, The Fooyin University, Ta-Liao, Kaohuing, Taiwan 831, R. O. C.*
[b]*Department of General Education, The Fooyin University, Ta-Liao, Kaohuing, Taiwan 831, R. O. C.*
[c]*Department of Applied Science, Chinese Naval Academy, 669, Jiun Shiaw Road, Kaohsiung, Taiwan 813, R. O. C.*

Received 17 August 2004; received in revised form 5 October 2004; accepted 5 October 2004
Available online 5 November 2004

Abstract

Two natural products, farformolide B and sesamin were isolated from *Farfugium japonicum* and *Cinnamomum kanehirae*, respectively. The structures of the two natural products, including their relative stereochemistry, were elucidated using spectroscopic data and theoretical calculations. The molecule 1 (farformolide B) is newly recognized by X-ray crystallography. The two compounds were also investigated by a theoretical analysis using the B3LYP/6-31G* method of the Gaussian 03 package program. The theoretical results were supplemented by experimental data to determine the optimal geometric structures of the two compounds. The calculated molecular mechanics were found to compare well with the experimental data. Several important thermodynamic properties of the two products, including ionization potentials, highest occupied molecular orbital (HOMO) and lowest unoccupied molecular orbital (LUMO) energies, energy gaps, heat of formation, atomization energies, and vibration frequencies, were also calculated. The study also provided a good understanding of the stereochemical structure and thermodynamic properties of the two molecules.

Keywords: Farformolide B; Sesamin; B3LYP; 6-31G*; Ionization potentials; HOMO and LUMO energies; Energy gaps; Heat of formation; Atomization energies; Vibration frequencies

1. Introduction

Many papers report that natural products play a highly significant role in the drug discovery and development process [1–5]. *Farfugium japonicum* is a plant commonly found in the shaded and humid surfaces of valleys or creek beds in Taiwan at elevations from a few hundreds to over a thousand meters high. There are few closely related species that often grow in such a great concentration. The whole plant and its underground stem can be used as herbal medicine with similar medical characteristics. The plant is effective in treating fever, continuous bleeding, and circulation enhancement. *Farfugium japonicum* tastes a little bitter and spicy, and farformolide B (**1**) was extracted from it.

Cinnamomum kanehirae is a special specie that is only found in Taiwan. The plant grows in the low elevations of the broad-leaf forest in Taiwan. The texture of its lumber is beautiful, and it is of high quality. Therefore, it is commonly used for carving. Sesamin (**2**) was isolated from the MeOH extract of *C. kanehirae*. Sesamin was obtained by systematic extraction and isolation from this plant. The lignans have an important role in plant defense, and they are also commercially employed as potent antioxidants. Sesamin is a major specie of lignan, and it strongly influences the lipid metabolism of experimental animals and humans. Sesamin shows that it causes a significant decrease in the activity and gene expression of hepatic fatty acid synthase and pyruvate kinase, the lipogenic enzymes [6]. Sesamin has been known

* Corresponding author. Tel.: +886 75834700; fax: +886 7 3472802.
E-mail address: ccsu@cna.edu.tw (C.-C. Su).

0301-4622/$ - see front matter © 2004 Elsevier B.V. All rights reserved.
doi:10.1016/j.bpc.2004.10.001

for many years as a highly resistant to oxidative deterioration [7]. Some scientists suggest that the people who result in senescent is caused by oxidation because the effect of oxidation may instigate the cell to decrepit or die. The oxygen molecule and other oxidizing agents in the body can apparently extract single electrons from the large molecules that make up cell membranes, thus making them very reactive. Subsequently, these activated molecules can link up and change the properties of the cell membrane. At some point, when enough of these reactions have occurred, the body's immune system comes to view the changed cell as an "enemy" and destroys it. Because of the worldwide trend to avoid or minimize the life of senile, the use of natural antioxidants is now receiving special attention.

Recently, there have been a number of experimental and theoretical studies of natural products, which includes NMR spectroscopy, mass spectroscopy, X-ray crystallographic, and molecular mechanics [8–23]. However, many of these theoretical studies involved only bond lengths and bond angles, but, commonly, these studies are not detailed thermodynamic properties or physical chemistry of the natural products. Correlation can be efficiently determined when the B3LYP methodology is used [24–37]. The B3LYP frequencies can be approached from experimental frequencies at medium basis set levels, and with even higher accuracy at large basis set levels. Some recent calculations have shown that using the B3LYP method together with the 6-31G* basis set function (BSF) of the density functional theory (DFT), which are included in the Gaussian 98 package program, can be a useful tool in providing accurate conformational analysis [38,39]. In order to understand the molecular mechanism of the two compounds, we also used the B3LYP/6-31G* method to determine the relative geometric structures, molecular orbital energy, and other thermodynamic properties of the two natural products in its ground state. The two natural products were selected to verify the accuracy of theoretical analysis vs. experimental results. The purpose of this research is also to help understand the absolute configuration and physical chemistry of the two natural products.

2. Experimental details

2.1. Reagents and chemicals

All chemicals used in this research were of available purity and were used without any further purification. Only analytical reagent grade chemicals were used in the preparation of the two natural products.

2.2. General apparatus

Optical rotations were measured with a JASCO DIP-370 digital polarimeter. UV spectra were obtained in MeOH using a JASCO V-530 spectrophotometer. Melting points were determined using a Yanagimoto micromelting point apparatus. The IR spectra were measured on a Hitachi 260-30 spectrophotometer. ^{1}H NMR (400 MHz) spectra (all in $CDCl_3$) were recorded with Varian NMR spectrometers, using TMS as an internal standard. LRFABMS and LREIMS spectra were obtained with a JEOL JMS-SX/SX 102 A mass spectrometer or a Quattro GC-MS spectrometer with a direct inlet system. Silica gel 60 (Merck, 230–400 mesh) was used for column chromatography. Precoated silica gel plates (Merck, Kieselgel 60 F-254, 0.20 mm) were used for analytical TLC, and precoated silica gel plates (Merck, Kieselgel 60 F-254, 0.50 mm) were used for preparative TLC.

2.3. Plant material

The plants were collected from Fooyin University, Kaohsiung Hsien, Taiwan in May, 2003. A voucher specimen was characterized by Dr. Horng-Liang Lay of the Graduate Institute of Biotechnology, National Pingtung University of Science and Technology, Pingtung County, Taiwan and deposited in the Fooyin University, Kaohsiung Hsien, Taiwan.

2.4. Extraction and isolation

F. japonicum (2.0 kg) was also extracted with MeOH. The extracts were concentrated in vacuo and partitioned between $CHCl_3$ and water. The organic layer was separated by silica gel column chromatography using gradient elution of $CHCl_3$-MeOH. Further purification by preparative TLC on silica gel with hexane-EtOAc (2:1) afforded a white powder of 43.0 mg farformolide B (**1**).

C. kanehirae were extracted with MeOH at room temperature repeatedly. The combined MeOH extracts (ca. 400 g) were evaporated and partitioned to yield $CHCl_3$ (ca. 250 g) and aqueous extracts. The $CHCl_3$ layer was further separated by column chromatography on Silica gel with gradients of *n*-hexane-EtOAc (4:1) to yield sesamin (**2**) (934.0 mg).

Farformolide B (**1**): Colorless needless. $C_{17}H_{26}O_5$, $[\alpha]_D^{25.4}$+186.7° (c 0.56, EtOAc). UV(MeOH)λ_{max} 234 nm. IR (Neat) V_{max} cm^{-1}: 3500, 2966, 1767, 1364, and 1073. EI-MS (70 eV) m/z (rel. int.%): 311 ([M+1]$^+$, 154 (100), 139 (47), 112 (33), 97 (45). ^{1}H-NMR (400 MHz, $CDCl_3$) δ: 0.80 (3H, d, J=6.4 Hz), 1.15 (3H, s), 1.16–1.26 (2H, m), 1.29–1.36, 1.54–1.60 (2H, m), 1.37–1.39 (2H, m), 1.39–1.41, 1.65–1.71 (2H, m), 1.95 (3H, s), 2.24, 2.33 (2H, d, J=14.4 Hz), 3.30 (3H, s), 3.34 (3H, s), and 4.20 (1H, s).

Sesamin (**2**): Colorless prism (hexane/EtOAc). $C_{20}H_{18}O_6$, $[\alpha]_D^{25}$+69.2° (c 0.56, EtOAc) , mp. 120–125 °C. ($CHCl_3$). UV λ_{max} (EtOH) nm: 209, 237, 287. IR v cm^{-1}: 950, 1040 (OCH_2O). EIMS m/z (rel. int.%):354 ([M]$^+$, 29.0), 203 (20.3), 178 (10.8), 161 (32.3), 150 (35.3), 149

(100), 135 (49.3), 131 (35.3), 122 (28.0), 121 (21.3), 117 (10.2), 115 (16.7), 103 (16.7), 91 (10.7), 77 (17.8), 65 (15.0), 63 (10.3). ^{1}H-NMR (400 MHz, $CDCl_3$) δ: 3.05 (2H, m), 3.86 (2H, dd, J=9.2, 3.6 Hz), 4.23 (2H, m), 4.71 (2H, d, J=4.4 Hz), 5.96 (4H, s), 6.78 (2H, d, J=8.4 Hz), 6.79 (2H, dd, J=8.4, 1.2 Hz), and 6.85 (2H, d, J=1.2 Hz).

2.5. Production of single crystals of the two natural products

Single crystals of the two natural products were produced by recrystallization followed by a crystal-growing process. The recrystallization involved heating the two natural products together with proper amount of hexane. Ethyl acetate was then slowly added to the mixture until dissolved. Magnesium sulfate was then added and the mixture was filtered while still hot. The filtered product was put into a crystal-growing bottle. Hexane vapor was used to slowly diffuse the product until a perfect crystal was produced. The structure of the resulting single crystals was analyzed by X-ray crystallography. Suitable crystals were selected and mounted on thin glass fibers using viscous oil. All measurements were made on a SMART CCD diffractometer with Mo Kα radiation (λ=0.7107 Å) at 295 K. The data were collected using the ω-step scan technique. The cell parameters were determined using all valid reflections. The intensity data were corrected for Lorentz and polarization effects, and refinement was made using the empirical absorption correction method based on equivalent reflections. The structures of the two natural products were solved by the direct methods and were refined by full-matrix, least-square data based on the F^2. The nonhydrogen atoms were refined anisotopically, and the hydrogen atoms were included in an idealized geometry but not refined. Atomic scattering factors and anomalous dispersion factors were determined using the SHELX program.

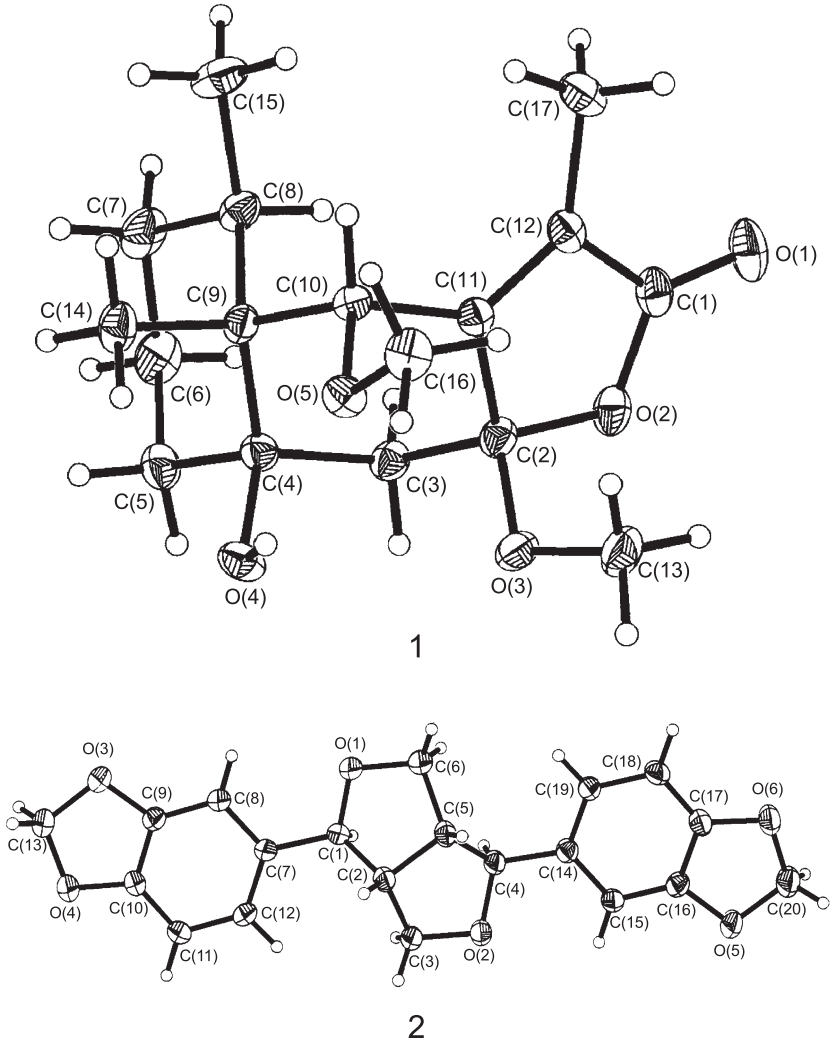

Fig. 1. ORTEP diagram of two natural products **1** and **2**.

3. Computational methods

3.1. Calculation methods and input

All calculations conducted in this research were performed using the B3LYP method included in the Gaussian 03 package program together with the 6-31G* basis set function of the density functional theory (DFT). The values obtained from the X-ray structural analysis were used as initial coordinates in the input to the program. The standard bond length, bond angle, and related atomic van der Waals radius were selected as starting point to conduct geometric optimization calculations. The objective is to accurately calculate the properties of the two natural products.

3.2. Geometry optimizations

The results of the calculations were used to verify the reasonableness of the input coordinate data. If unreasonable data were used, either the geometric symmetry of the molecules would be destroyed or unusual bond length or bond angle would be produced. Any of these errors would result in the termination of the calculations. It was found that calculation convergence could be much easily achieved if the input data were closer to the experimental minimal energy points of the molecules. By starting the calculations using the X-ray structural analysis of coordinates, the convergence of the Self-Consistent Field (SCF) calculations were achieved in fewer steps. The optimal geometric bond length, bond angle, and dihedral angle of the two natural products were obtained from the converged calculation results.

3.3. Procedure of orbital field energy, vibration frequency and thermodynamic properties of measurements

Using the optimization of the geometric calculations, thermodynamic properties such as orbital energy, vibration frequency, ionization energy, energy gap between highest occupied molecular orbital (HOMO) and lowest unoccupied molecular orbital (LUMO), atomic heat, enthalpy, Gibbs energy, etc., of each of the two natural products

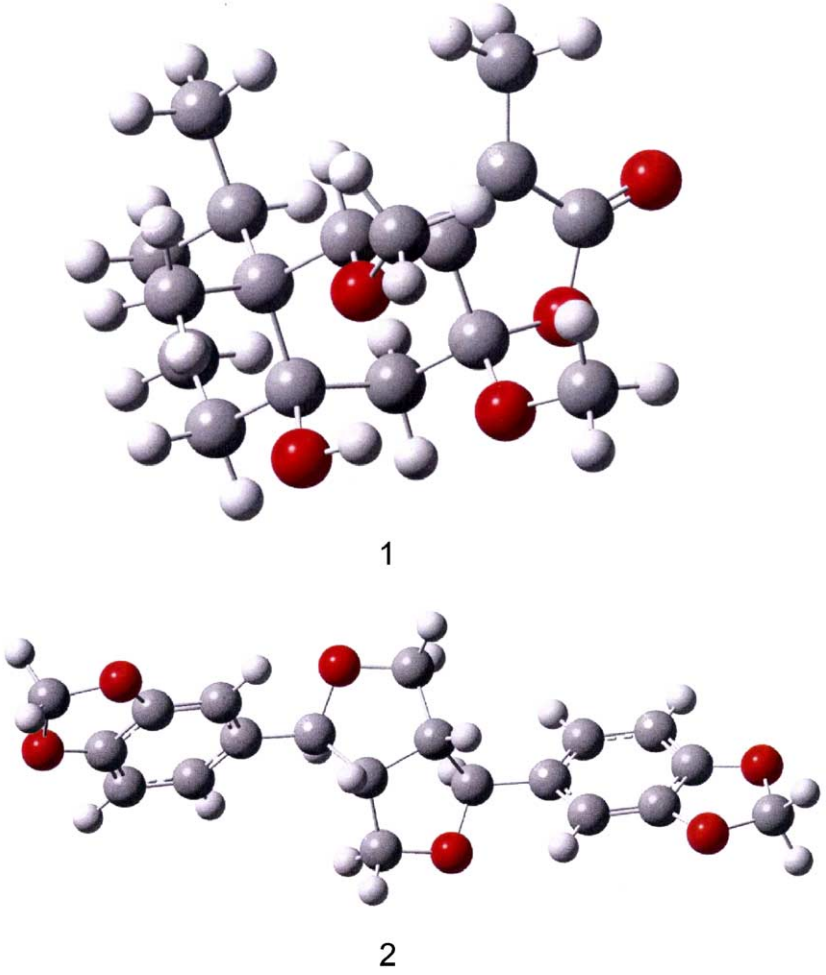

Fig. 2. Theoretical calculation diagram of two natural products **1** and **2**.

were obtained. Vibration frequencies of the products were also calculated at the B3LYP/6-31G* level mainly to check the number of imaginary frequencies and to calculate the zero-point energies. The results were then used to determine the relative stability of the two natural products. The resulting molecular stability, conductivity, and thermodynamic properties are of special importance and value.

4. Results and discussions

4.1. Geometric structure

Through structural analysis using X-ray crystallography, the ORTEP diagrams of the two natural products were also identified, as shown in Fig. 1. Theoretical calculations obtained geometric structures of the two natural products are shown in Fig. 2. It is known that stereochemical structure is involved in antioxidant or antibacterial arena. We have found natural product **1** having a lactone at the C-1 position in its structure. Similarly, natural product **2** was found to have six epoxides in its structure. The theoretical studies of the two natural products confirmed the X-ray analysis. As described earlier, the coordinates of the X-ray structural analysis were used as input to the calculation program for comparing the reliability and reasonableness of the theoretical methods used in this research. The AM 1 semiempirical method was first used to conduct calculations until convergence was achieved. The geometry optimization was then conducted using the 6-31G* BSF and the B3LYP method. The two natural products were found to locate the local minima of the potential energy surface at the B3LYP/6-31G*. Tables 1 and 2 provide the resulting bond

Table 1
Selected crystallographic data and optimized structure of compound **1** located using B3LYP/6-31G* calculations for atomic bond lengths (Å) and bond angles (°) with slightly larger differences (atomic bond length differences greater than 0.01 Å and atomic bond angle greater than 1°)

	Crystallographic data	B3LYP/6-31G*
Atomic bond lengths (Å)		
O2–C1	1.365	1.375
O2–C2	1.453	1.443
C1–C12	1.468	1.494
C2–C11	1.498	1.519
C2–C3	1.513	1.527
C3–C4	1.543	1.556
C4–C5	1.530	1.540
O4–C9	1.570	1.590
C5–C6	1.512	1.531
C6–C7	1.512	1.531
C7–C8	1.534	1.545
C9–C10	1.551	1.572
C11–C12	1.331	1.341
Atomic bond angles (°)		
C16–O5–C10	112.5	113.8
O1–C1–O2	121.2	122.9
O1–C1–C12	129.6	128.4
O3–C2–C11	116.9	115.5
C2–C3–C4	114.1	113.0
C8–C9–C4	108.6	109.7
C11–C12–C17	130.4	132.2
C1–C12–C17	121.7	120.1

Table 2
Selected crystallographic data and optimized structure of compound **2** located using B3LYP/6-31G* calculations for atomic bond lengths (Å) and bond angles (°) with slightly larger differences (atomic bond length differences greater than 0.01 Å and atomic bond angle greater than 1°)

	Crystallographic data	B3LYP/6-31G*
Atomic bond lengths (Å)		
O1–C1	1.413(3)	1.428
O2–C3	1.415(4)	1.430
C2–C3	1.504(4)	1.543
C7–C8	1.396(3)	1.412
C9–C10	1.378(3)	1.395
C11–C12	1.391(4)	1.408
C16–C17	1.375(4)	1.394
C18–C19	1.396(4)	1.408
O4–C13	1.411(3)	1.432
O5–C20	1.421(4)	1.431
O6–C20	1.416(3)	1.432
C1–C2	1.513(3)	1.552
C2–C5	1.541(3)	1.546
C4–C5	1.517(4)	1.552
C10–C11	1.362(4)	1.379
C14–C19	1.383(3)	1.397
C15–C16	1.359(4)	1.378
C17–C18	1.363(4)	1.379
Atomic bond angles (°)		
C1–O1–C6	107.1(2)	108.0
C8–C7–C1	120.9(2)	119.5
C3–O2–C4	105.7(2)	108.0
C10–O4–C13	106.4(2)	105.5
O1–C1–C2	105.1(2)	104.1
C14–C4–C5	117.8(2)	115.5
C4–C5–C6	114.5(3)	116.6
O1–C6–C5	105.6(3)	107.1
C12–C7–C1	119.3(2)	120.2

Table 3
Selected crystallographic data and optimized structure of compound **1** located using B3LYP/6-31G* calculations for dihedral angles (°) with larger differences

Dihedral angles (°)	Crystallographic data	B3LYP/6-31G*
C1–O2–C2–O3	−129.3	−122.9
C13–O3–C2–O2	49.6	55.0
C13–O3–C2–C11	−68.8	−62.4
C16–O5–C10–C9	76.9	86.3
O3–C2–C3–C4	81.2	73.7
O3–C2–C11–C10	−72.3	−67.2
C3–C2–C11–C10	48.0.	53.2
C4–C5–C6–C7	−69.1	−53.5
C7–C8–C9–C4	68.9	53.2
C7–O8–C9–C19	−59.0	−68.6
C15–C8–C9–C14	50.7	55.8
O5–C10–C11–C2	60.3	67.8
O5–C10–C11–C12	131.3	120.8
C9–C10–C11–C2	−63.5	53.2
C9–C10–C11–C12	104.8	118.2

Table 4
Selected crystallographic data and optimized structure of compound **2** located using B3LYP/6-31G* calculations for dihedral angles (°) with larger differences

Dihedral angles (°)	Crystallographic data	B3LYP/6-31G*
C3–O2–C4–C14	169.0	162.7
C13–O3–C9–C10	−1.4	−8.0
C9–O3–C13–O4	2.3	13.0
C13–O4–C10–C9	1.6	8.1
C10–O4–C13–O3	−2.4	−13.0
O1–C1–C7–C8	10.8	−40.4
O1–C1–C7–C12	−171.9	141.7
C2–C1–C7–C8	133.0	77.1
C2–C1–C7–C12	−49.6	−100.8
O2–C4–C14–C15	25.3	−39.3
O2–C4–C14–C19	−159.5	142.9
C5–C4–C14–C15	143.6	78.2
C5–C4–C14–C19	−41.2	−99.5

lengths and bond angles of the two natural products from selected both the X-ray crystallography structural analysis and theoretical calculations with slightly large differences. Tables 3 and 4 list the dihedral angles obtained from selected both the X-ray crystallography analysis and theoretical calculations with large differences. As a result, the average difference is small in experimental and theoretical calculation. Table 5 provides the crystallographic data collected during the study. Appropriate fitness between the overall calculated and experimental structures of the two natural products can be seen in the results.

Table 5
Crystallographic data

	1	**2**
Empirical formula	$C_{17}H_{26}O_5$	$C_{20}H_{18}O_6$
Formula weight	310.38	354.34
Crystal system	Monoclinic	Monoclinic
Space group	P2(1)	P2(1)
Unit cell dimensions (Å)	*a*=7.1982(5)	*a*=9.9723(8)
	b=12.8985(9)	*b*=6.9509(6)
	c=9.3138(7)	*c*=11.8965(10)
B (°)	108.889(2)	93.696
Volume (Å^3)	818.18(10)	822.91(12)
Z (atoms/unit cell)	2	2
Dcalc/mg m^{-3}	1.260	1.430 mg/m^3
T (K)	295(2)	295(2)
Absorption coefficient	0.091	0.106
F(000)	336	372
θ range (deg)	2.31 to 27.50	1.72 to 27.50
Crystal size	0.28×0.25×0.07 (mm^3)	0.40×0.40×0.25 (mm^3)
Index ranges	*h* (−9 to 9)	*h* (−12 to 12)
	k (−16 to 16)	*k* (−6 to 9)
	l (−12 to 10)	*l* (−15 to 15)
Reflection collection	8014	7330
Independent reflection	3749 (*R*(int)=0.0243)	3330 (*R*(int)=0.0268)
Absorption correction	empirical	empirical
Max. and min. transmission	0.9936 and 0.9748	0.9740 and 0.9588
Data/restraints/parameters	3749/1/99	3330/1/236
GOF on F^2	1.085	1.011
Final *R* indices [$I>2\sigma(I)$]	R1=0.0590	R1=0.0555
	WR2=0.1483	WR2=0.1525
R indices(all data)	R1=0.0676	R1=0.0630
	WR2=0.1555	WR2=0.1608
Largest difference peak/hole[e Å^{-3}]	0.245/−0.193	0.393/−0.265

Table 6
Comparison of HOMO, LUMO, energy gaps ($\Delta\varepsilon_{HOMO-LUMO}$), and first ionization potentials of the two compounds (eV)

Molecule parameter	ε_{HOMO}	ε_{LUMO}	I_{1st}	$\Delta\varepsilon_{HOMO-LUMO}$
1	−6.7984	−1.4144	6.7984	5.3840
2	−5.5832	−0.0735	5.5832	5.5097

4.2. Molecular first ionization potentials, HOMO and LUMO energies, energy gaps

Table 6 lists the calculated values of the first ionization potentials, HOMO, LUMO, and energy gap ($\Delta\varepsilon_{HOMO-LUMO}$) of the two natural products. Table 6 also shows that natural product **2** has higher first ionization potential.

4.3. Thermodynamic properties: ΔH_f, ΔG_f, ΔH_a, ΔG_a

Table 7 lists the calculated thermodynamic properties of the two natural products, including enthalpy of formation (ΔH_f), Gibbs energy of formation (ΔG_f), enthalpy of atomization (ΔH_a), and Gibbs energy of atomization (ΔG_a). These thermodynamic data provide information about the relative stabilities of the two natural products. In general, the formation of the two natural products is found to be exothermic ($\Delta H<0$). The entropy change of the reaction is also found to be slightly negative. However, the change in enthalpy is found to be big and negative enough to overcome the negative change of entropy. These calculated results show the two products having negative Gibbs energy of formation ($\Delta G_f<0$), indicating that the two natural products are stable and are easy-to-form molecules.

4.4. Vibration frequencies

Through vibration frequency studies, the two natural products can reveal the features of two molecules. The carbonyl bond with no formation of hydrogen bonding, its vibration frequency is approximately 1700 cm^{-1} ($\nu_{C=O}$). After the hydrogen-bond formation, hydrogen atom is to bind another functional group of oxygen. Therefore, it will decrease the strength of carbonyl bond, force constant, and vibration frequency. The

Table 7
Comparison of calculated Thermodynamic properties of the two compounds (298 K, kcal mol^{-1})

Molecule parameter	ΔH_f	ΔG_f	ΔH_a	ΔG_a
1	−2172.14	−1945.94	4735.154	4332.91
2	−2451.80	−2237.74	4815.58	4438.34

carbonyl bond vibration frequencies of the natural product **1** in theoretical calculation and infrared spectrometry were 1746 and 1767 cm^{-1}, respectively. The calculated vibration frequencies of the two natural products are all positive, indicating that the two molecules are at the minimal points of the potential energy surfaces and therefore are very stable molecules. The calculated maximum frequencies of the two products are between 3701.573 and 3238.165 cm^{-1}. Natural product **2** is also found to have lower frequency (11.150 cm^{-1}).

5. Concluding remarks

Two natural products were isolated and their absolute stereochemical configurations were determined. Through the theoretical calculations using the B3LYP/6-31G* density functional method, data of the two natural products were successfully obtained. From these, calculated and analytical results can be summarized as follows:

(1) The calculated bond lengths and torsion angles of the two natural products are very close to the experimental values and are quite reasonable. The optimized geometries were determined. The calculated results were found to be close to the experimental data obtained from X-ray crystallography. The calculations of geometric structures of two molecules appear to be successful.
(2) Through the calculations of the first ionization potentials, HOMO, LUMO, and energy gaps, it was found that the two natural products have low energy gaps between the first ionization potentials and HOMO.
(3) The calculations of thermodynamic properties and vibration frequencies show that the two natural products are all located at the stable, minimal points of the potential energy surfaces. They are all therefore stable natural products. According to former calculated results, molecule that has larger positive value of vibration frequency is more stable and not easy to be cracked. Because of the larger frequency and molecular stability, the natural product **1** is not easy to decompose than natural product **2**. Natural product **2**, having the lower frequency, is significant because it represents its having a weaker bond than natural product **1**.

The calculations using the B3LYP DFT and 6-31G* BSF have also shown satisfactory results in both accuracy and execution time. Good agreement between theoretical and experimental structures was also found. This combined study should provide contribution to the natural products-based drug in pharmaceutical discovery and other related fields. Accurate theoretical calculations can help identify and provide ways to obtain important chemical and physical information that cannot be easily obtained by experimental approaches.

Acknowledgement

The authors thank the National Science Council of the Republic of China (Taiwan) for its financial support (NSC 92-2321-B-242-001). Dr. Y.C. Su, P.E., of Houston, Texas, USA, is also appreciated for a critical reading of this manuscript.

References

[1] F. Deanda, K.M. Smith, J. Liu, R.S. Pearlman, Mol. Pharmacol. 1 (2003) 23–39.
[2] Zaheer-ul-haq, B. Wellenzohn, K.R. Liedl, B.M. Rode, J. Med. Chem. 46 (2003) 5087–5090.
[3] D.J. Newman, G.M. Cragg, K.M. Snader, J. Nat. Prod. 66 (2003) 1022–1037.
[4] B. Jaki, O. Sticher, R. Fröhlich, G.F. Pauli, J. Nat. Prod. 65 (2002) 517–522.
[5] E.A. Amin, W.J. Welsh, J. Med. Chem. 44 (2001) 3849–3855.
[6] M. Kusiro, T. Massoka, S. Hageshita, Y. Takahashi, T. Ide, M. Sugano, J. Nutr. Biochem. 13 (2002) 289–295.
[7] A. Mohamed, I.I. Awatif, Food Chem. 62 (1998) 269–276.
[8] R.D. Frin, C.G. Jones, Nat. Prod. Rep. 20 (2003) 382–391.
[9] P.G. Williams, W.Y. Yoshida, M.K. Quon, R.E. Moore, V.J. Paul, J. Nat. Prod. 66 (2003) 1545–1549.
[10] C.L. Cardoso, D.H.S. Silva, D.M. Tomazeia, H. Verli, M.C.M. Young, M. Furian, M.N. Eberlin, V. da Silva Bolzani, J. Nat. Prod. 66 (2003) 1017–1021.
[11] P. Iturriaga-Vásquez, R. Miquel, M.D. Ivorra, M.P. Dócon, B.K. Cassels, J. Nat. Prod. 66 (2003) 954–957.
[12] P. Wipf, A.D. Keres, J. Nat. Prod. 66 (2003) 716–718.
[13] J.F. Rivero-Cruz, M. Macías, C.M. Cerda-Carcía-Rojas, R. Mata, J. Nat. Prod. 66 (2003) 511–514.
[14] L.U. Romān, C.M. Cerda-García-Rojas, R. Guzmán, C. Armenta, J.D. Hernández, P. Joseph-Nathan, J. Nat. Prod. 65 (2002) 1540–1546.
[15] E. Harvala, N. Aligiannis, A.-L. Skaltsounis, H. Pratsinis, K. Lambrinidis, C. Harvla, J. Nat. Prod. 65 (2002) 1045–1048.
[16] B. Jaki, O. Sticher, V. Markus, R. Fröhlich, G.F. Pauli, J. Nat. Prod. 65 (2002) 517–522.
[17] E.A. Amin, W.J. Welsh, J. Med. Chem. 44 (2001) 3849–3855.
[18] M.J. Comin, J.B. Rodriguez, Tetrahedron 56 (2000) 4639–4649.
[19] S. Gibbons, B.J. Denny, S. Ali-Amine, K.T. Mathew, B.W. Skelton, A.I. Gray, J. Nat. Prod. 63 (2000) 839–840.
[20] A.F. Barrero, J.E. Oltera, I. Rodriguez-García, A. Barragán, M. Álvatez, J. Nat. Prod. 63 (2000) 305–307.
[21] M.S. Maier, D.I.G. Marimon, C.A. Stortz, M.T. Adler, J. Nat. Prod. 62 (1999) 1565–1567.
[22] F.J. Devlin, P.J. Stephens, J.R. Cheeseman, M.J. Frisch, J. Phys. Chem., A 101 (1997) 6322–6333.
[23] Y. Uesugi, M. Mizuno, A. Shimojima, H. Takahashi, J. Phys. Chem., A 101 (1997) 268–274.
[24] T.C. Ramalho, R.D. de Alencastro, M.A. La-Scalea, J.D. Figueroa-Villar, Biophys. Chem. 110 (2004) 267–279.
[25] Q.A. Qiao, Z.T. Cai, D.C. Feng, Y.S. Jiang, Biophys. Chem. 110 (2004) 259–266.
[26] J.M. Granadino-Roldán, M. Fernández-Gómez, A. Navarro, T.P. Ruiz, U.A. Jayasooriya, Phys. Chem. Chem. Phys. 6 (2004) 1133–1143.
[27] D. Troyz, R.Z. Pascual, G.C. Schatz, J. Phys. Chem., A 107 (2003) 10497–10506.

[28] W. Chen, Y. Lam, M.W. Wong, H.H. Huang, E. Liang, J. Phys. Chem., A 107 (2003) 6714–6719.
[29] R. Schurhammer, P. Vayssière, G. Wipf, J. Phys. Chem., A 107 (2003) 11128–11138.
[30] K. Sung, F.-L. Chen, Org. Lett. 5 (2003) 889–891.
[31] M. Domagala, S.J. Grabowski, K. Urbaniak, G. Mloston, J. Phys. Chem., A 107 (2003) 2730–2736.
[32] Y. Shiota, N. Kihara, T. Kamachi, K. Yoshizawa, J. Org. Chem. 68 (2003) 3958–3965.
[33] S. Gustavsson, A. Rosén, K. Bolton, Nano Lett. 3 (2003) 265–268.
[34] J.J. Queralt, J. Andrés, C.L. Moisés, J.H. Cobas, J.A. Santaballa, J.R. Sambrano, Chem. Phys. 280 (2002) 1–14.
[35] Y. Sheng, J. Leszczynski, J. Phys. Chem., A 106 (2002) 12095–12102.
[36] R. Ida, G. Wu, J. Phys. Chem., A 106 (2002) 11234–11239.
[37] M. Bendikov, Y. Apeloig, S. Bukalov, I. Garbuzova, L. Leites, J. Phy. Chem., A 106 (2002) 4880–4885.
[38] C.C. Su, L.H. Lu, L. Liu-Kao, J. Phys. Chem., A 107 (2003) 4563–4567.
[39] C.C. Su, L.H. Lu, J. Mol. Struct. 702 (2004) 23–31.